

Tuning ice nucleation with counterions on polyelectrolyte brush surfaces

Zhiyuan He,^{1*} Wen Jun Xie,^{2*} Zhenqi Liu,¹ Guangming Liu,³ Zuowei Wang,⁴ Yi Qin Gao,^{2†} Jianjun Wang^{1†}

2016 © The Authors, some rights reserved; exclusive licensee American Association for the Advancement of Science. Distributed under a Creative Commons Attribution NonCommercial License 4.0 (CC BY-NC). 10.1126/sciadv.1600345

Heterogeneous ice nucleation (HIN) on ionic surfaces is ubiquitous in a wide range of atmospheric aerosols and at biological interfaces. Despite its great importance in cirrus cloud formation and cryopreservation of cells, organs, and tissues, it remains unclear whether the ion-specific effect on ice nucleation exists. Benefiting from the fact that ions at the polyelectrolyte brush (PB)/water interface can be reversibly exchanged, we report the effect of ions on HIN on the PB surface, and we discover that the distinct efficiency of ions in tuning HIN follows the Hofmeister series. Moreover, a large HIN temperature window of up to 7.8°C is demonstrated. By establishing a correlation between the fraction of ice-like water molecules and the kinetics of structural transformation from liquid- to ice-like water molecules at the PB/water interface with different counterions, we show that our molecular dynamics simulation analysis is consistent with the experimental observation of the ion-specific effect on HIN.

INTRODUCTION

Ice formation is ubiquitous and crucial in many fields such as cryobiology, geology, and climate science (1–4). It is believed that the molecular-level understanding of ice formation is essential to predict the future of our planet (5–7). Ions are often involved in the process of ice formation (8–12). Early studies showed that the growth rate of ice in aqueous alkali halide solutions is strongly dependent on the type of salts (8–10). It might be due to the differential incorporation of ions in the ice crystals or selective adsorption of ions at the ice/water interface (11, 12). Particular interests have been focused on ice nucleation because it is the initial and rate-limiting step for ice formation (3, 4, 13–15). Pruppacher and Neuberger (16) and Pruppacher (17) studied the relationship between the supercooling and the structure of aqueous solutions with monovalent ions and found that the nonequilibrium freezing point depression of a solution varied with the type of salts and, for a particular salt, increased with the salt concentration. Recently, Koop *et al.* (18) revealed that homogeneous ice nucleation in an aqueous solution could be predicted by water activity. Thermodynamic anomalies of water crystallization were investigated by Moore and Molinero (19) and Hudait and Molinero (20), who found that the fraction of four coordinated molecules in supercooled liquid water controlled the ice nucleation rate. However, in real systems, ice nucleation occurs more often on foreign surfaces, that is, through heterogeneous ice nucleation (HIN). For example, Ehre *et al.* (2) and Belitzky *et al.* (21) found that HIN on charged surfaces was affected by the interfacial water structure, which was also dependent on the amount of surface charges. Abbatt *et al.* (22) discovered that HIN on the surface of solid ammonium sulfate aerosols was a pathway for the formation of cirrus cloud, which could cover up to 30% of Earth's atmosphere and greatly affect the global climate. Therefore, it is highly desirable to investigate the effect of ions on HIN.

Although very few theoretical and experimental studies on the ion specificity of HIN have been conducted, the ion-specific effects on the

dynamics and structure of interfacial water and other related surface phenomena have been studied for many years (18, 23–27). One pioneering study is the discovery of the Hofmeister series in which ions are ranked according to their ability in salting out proteins from aqueous solutions (28). Note that the Hofmeister series of ions explains many surface phenomena in chemistry and biology (29–32). Recent reports have shown that counterions at various ionic surfaces control the dynamics and structure of interfacial water (23, 33–35). Such observations lead to a reasonable speculation that counterions on solid surfaces can affect HIN because the theoretical analysis shows that the structure transformation in water determines HIN (33–35). Although the prediction is reasonable, it remains an open question whether the ion-specific effect exists for HIN on ionic surfaces.

Here, we investigate HIN on polyelectrolyte brush (PB) surfaces. The PB consists of densely end-grafted polyelectrolyte chains, carrying a large number of ionic groups, as shown in Fig. 1. The reversible exchange of counterions in the PB has been explored for a variety of applications, such as designing surfaces with tunable wettability and friction (24, 36–38). Furthermore, the embedded counterions in the PB can provide a unique microenvironment and have been used as carriers for proteins and microreactors to fabricate nanoparticles with high catalytic activity (39, 40). When a drop of pure liquid water is placed atop the PB surface, a fraction of counterions will be released from the PB due to the osmotic pressure, forming a diffusion layer of counterions at the brush/water interface (13, 41). Therefore, the PB surface provides an ideal platform for the investigation of the ion-specific effect on ice nucleation atop ionic surfaces. We have found that HIN can be tuned by exchanging the counterions of the PB, and the distinct efficiency of ions in tuning HIN follows the Hofmeister series. Such phenomena can be well interpreted by the molecular dynamics (MD) simulation analysis. The diffused counterions at the brush/water interface can effectively regulate the dynamics and structure of interfacial water and thus determine the HIN process.

RESULTS

HIN of water drops on the PB surfaces with different counterions was signified by a sudden change in opacity before and after freezing

¹Key Laboratory of Green Printing, Institute of Chemistry, Chinese Academy of Sciences, Beijing 100190, China. ²Beijing National Laboratory for Molecular Sciences, Institute of Theoretical and Computational Chemistry, College of Chemistry and Molecular Engineering, Peking University, Beijing 100871, China. ³Department of Chemical Physics, Hefei National Laboratory for Physical Sciences at the Microscale, University of Science and Technology of China, Hefei 230026, China. ⁴School of Mathematical and Physical Sciences, University of Reading, Whiteknights, Reading RG6 6AX, UK.

*These authors contributed equally to this work.

†Corresponding author. Email: wangj220@iccas.ac.cn (J.W.); gaoyq@pku.edu.cn (Y.Q.G.)

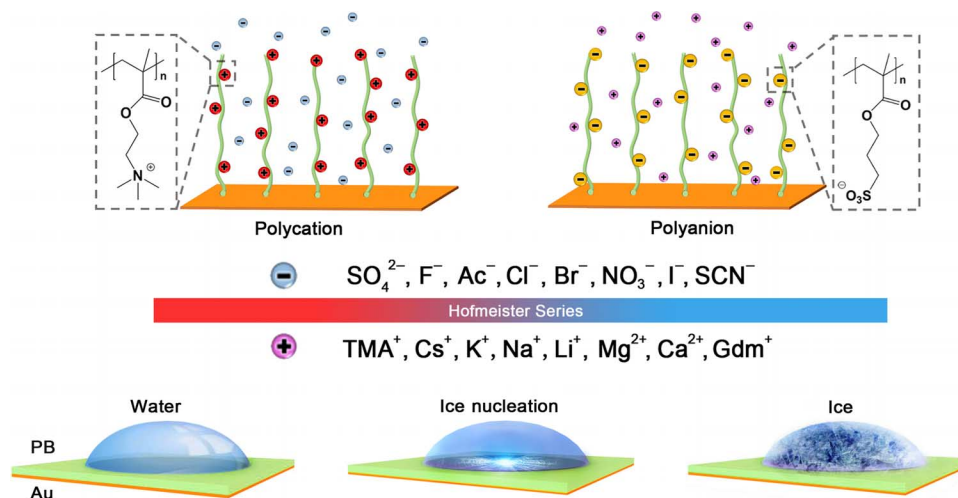


Fig. 1. Illustration of HIN on cationic and anionic PB surfaces with different counterions. Cationic poly[2-(methacryloyloxy)-ethyltrimethylammonium] (PMETA) and anionic poly(3-sulfopropyl methacrylate) (PSPMA) brushes are used to study the effect of diffused counterions on tuning HIN. The counterions on the PMETA and PSPMA brush surfaces can be successfully exchanged by immersing the brush surface into a solution containing expected counterions (fig. S1).

(Fig. 1 and fig. S2) (42). The freezing process of a water drop includes ice nucleation and ice growth, with the former being the rate-limiting step (19). Ice formation in the water drop started at the brush/water interface, followed by the upward ice growth (Fig. 1 and fig. S3). Upon the formation of ice nucleus, ice grew spontaneously, and the whole drop turned into ice within 0.5 s.

As shown in Fig. 2A (1 to 3), the HIN temperature (T_H) on the PMETA-I brush surface (0.05 chain/nm^2) is -23.8°C , whereas it is -26.4°C on exactly the same brush surface but with SO_4^{2-} as the counterion (fig. S4). Note that we can reversibly tune the T_H on the PB surface through cycling the counterion exchange, as demonstrated in Fig. 2B. Consecutively replacing I^- with SO_4^{2-} of the PMETA led to a dropping of the T_H from $-23.5 \pm 0.4^\circ\text{C}$ to $-26.5 \pm 0.3^\circ\text{C}$ and vice versa. Another significant advantage of the PB over many other materials, such as surfactant micelles, is that its thickness and grafting density can be easily controlled, which can lead to a much broader range of T_H . We then prepared a series of PMETA brush surfaces with the grafting density (σ) varied from 0.03 to 0.50 chain/nm^2 . The T_H of water drops on PMETA- SO_4 , PMETA-Cl, and PMETA-I brush surfaces with various grafting densities is shown in Fig. 2C. At each given grafting density, the T_H increases in the same order as $\text{SO}_4^{2-} < \text{Cl}^- < \text{I}^-$. On the other hand, for the PB surfaces consisting of the same type of counterion, the T_H increases with the grafting density. The T_H is $-26.5 \pm 0.3^\circ\text{C}$ on the PMETA- SO_4 brush surface with a grafting density of 0.05 chain/nm^2 and is $-18.7 \pm 0.6^\circ\text{C}$ on the PMETA-I brush surface with a grafting density of 0.50 chain/nm^2 , exhibiting a T_H window as large as 7.8°C , as shown in Fig. 2C.

We next studied the ion-specific effect as a function of the brush thickness. When the PMETA brush height is increased from 2 to 50 nm (measured in air) at a fixed grafting density of 0.50 chain/nm^2 , the differences among the T_H on the PMETA- SO_4 , PMETA-Cl, and PMETA-I surfaces are significantly amplified, whereas the order remains the same, as shown in Fig. 2D. The absence of ion-specific effect on PMETA brush surfaces with a low thickness of 2 nm was also verified by investigations of HIN on the NMe_3^+ -terminated self-assembled monolayers (SAMs) with various counterions (fig. S6)

(29). The absence of ion specificity in HIN should be related to the low concentration of diffused ions at the interfaces, which agrees with other ion-specific phenomena (29, 43). The influence of the cooling rate (from 1.0 to 10.0°C/min) in the T_H was also studied, and the trend of the ion-specific effect on HIN is the same, as shown in fig. S7.

To have a more complete series of ions on tuning HIN, we investigated the HIN on the PMETA brush surfaces with a large variety of counteranions, as shown in Fig. 3A. The T_H increases in the anion sequence of $\text{SO}_4^{2-} < \text{F}^- < \text{Ac}^- < \text{HPO}_4^{2-} < \text{Cl}^- < \text{Br}^- < \text{SCN}^- < \text{NO}_3^- < \text{I}^-$, which matches well with the Hofmeister series. To further consolidate the specific effect of anion on HIN, we studied the corresponding nucleation delay time (t_D) at -20.0°C (details in Materials and Methods), which varied from 5 to 6500 s with the change of anions, as shown in Fig. 3B. The decrease of t_D is consistent with the increase of T_H . Cation-specific effect on HIN was also studied on poly(3-sulfopropyl methacrylate potassium) (PSPMA) brush surfaces as well as SO_3^- -terminated SAMs with different counteranions for comparison. The T_H of water droplets (Fig. 3C and fig. S8) on PSPMA brush surfaces with different cations shows the order of $\text{Ca}^{2+} < \text{Mg}^{2+} < \text{Gdm}^+ < \text{K}^+ < \text{Na}^+ < \text{Cs}^+ < \text{TMA}^+ < \text{Li}^+ < \text{NH}_4^+$, which is further confirmed by the results of t_D (Fig. 3D). The sequence of cations is roughly in accordance with the previously proposed Hofmeister series in affecting other properties (29). In contrast, we did not observe ion-specific effect for HIN on SO_3^- -terminated SAM surfaces (fig. S9). In general, the Hofmeister series is more pronounced in anions than in cations (44). Thus, we elucidated the ion-specific effect for HIN on model systems of PMETA brush surfaces with different counteranions.

The ion-specific effects on HIN do not explicitly correlate to the change of the macroscopic properties of the PB, such as wettability, viscoelasticity, roughness, or swelling/collapsing behavior, upon the variation of counterions (more details in figs. S10 to S13). To gain molecular-level insight into the ion specificity in tuning HIN, we performed MD simulations to study the ion-specific effect on the structure and dynamics of interfacial water (in fig. S14) (19, 45). Three halide counterions (F^- , Cl^- , and I^-) were chosen as representatives

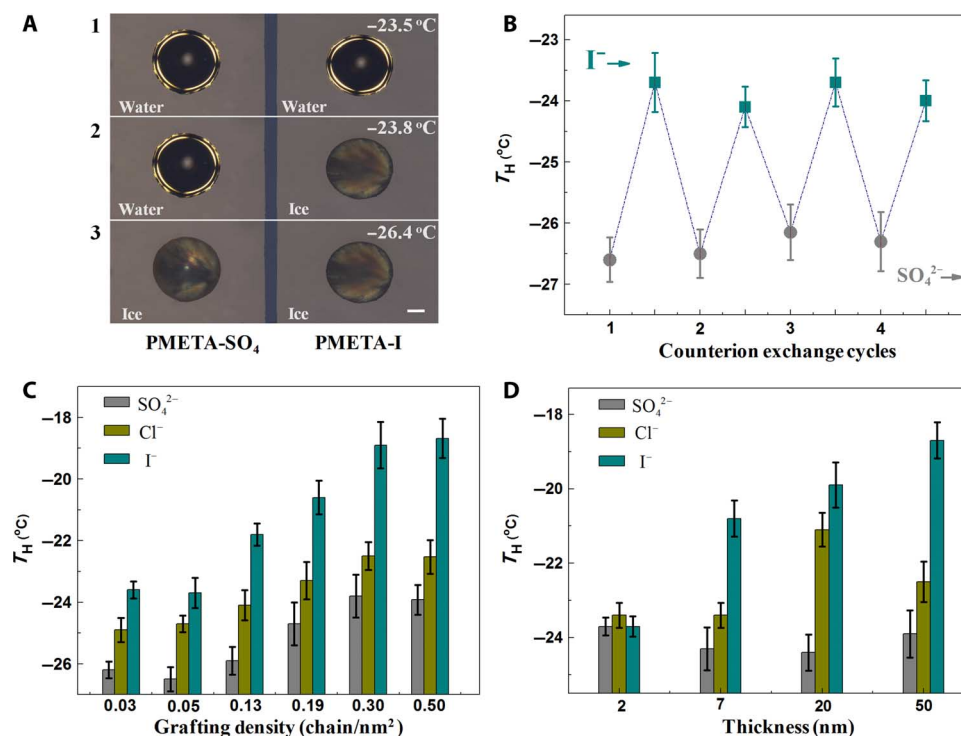


Fig. 2. T_H on the PMETA brush surfaces. (A) Polarized optical microscopic images of water drops before (1) and after (3) freezing on PMETA-SO₄ and PMETA-I brush surfaces (on the same wafer; in fig. S4). The PMETA-SO₄ and PMETA-I brush surfaces exhibited distinct T_H . Scale bar, 200 μm . (B) Reversible switch of the T_H of water drops on the PMETA brush surfaces through the consecutive counterion exchange of Γ^- and SO_4^{2-} (0.05 chain/nm²). (C and D) The influence of grafting density (C) and thickness (D) (fixed grafting density of 0.50 chain/nm²) on the T_H of PMETA-SO₄, PMETA-Cl, and PMETA-I brush surfaces. The measurements were carried out in a closed chamber with a relative humidity of 100%, and the samples were chilled from room temperature to -50.0°C with a cooling rate of $2.0^\circ\text{C}/\text{min}$. All experimental results on the T_H were based on more than 200 freezing events for each PMETA-SO₄, PMETA-Cl, and PMETA-I brush surfaces (in fig. S5).

in the Hofmeister series, in which Cl^- situates in the middle and F^- and Γ^- belong to the two ends. The PMETA brush swells in water, and its counterions can diffuse into the surrounding water [above the outermost quaternary ammonium-positive (QA^+) group]. The diffused halide anions are defined as the ions at the brush/water interface that are not in direct contact with any outmost QA^+ groups. As shown in Fig. 4A, an important feature is that the concentrations of all three counterions approach zero at about 15 \AA away from the outmost QA^+ group (fig. S15). The numbers of the diffused counterions of F^- , Cl^- , and Γ^- at the brush/water interface differ significantly, and the concentration of F^- is almost three times that of Γ^- . MD simulations at different temperatures further confirmed this finding (fig. S16). The electric fields at the brush/water interface (with the magnitude of 100 to 1000 $\text{kV} \cdot \text{cm}^{-1}$), induced by the diffused counterions, are shown in fig. S17. The intensity of the electric field increases in the same order as the ionic concentration $\Gamma^- < \text{Cl}^- < \text{F}^-$, and both follow the Hofmeister series. However, the intensity of electric field is far below the required value ($\sim 10,000 \text{ kV} \cdot \text{cm}^{-1}$) for inducing ice nucleation, and so plays a minor role in the observed HIN (21, 46). To gain more insights into the underlying molecular mechanism of this ion-specific effect on HIN, we calculated the dynamics and structure of the interfacial water (in MD method and fig. S18) (47). We found that the fraction of ice-like water molecules (tetrahedrality above 0.9; in MD method and Fig. 4B) typically increases in the order of $\text{F}^- < \text{Cl}^- < \Gamma^-$.

The diffused counterions at the brush/water interface also have a profound ion-specific effect on the relaxation of OH bond orientation and the formation rate of ice-like water molecules. The orientation of interfacial water molecules relaxes in the order of $\text{F}^- < \text{Cl}^- < \Gamma^-$ because anions with high charge density (F^- , in this case) tend to slave the surrounding water molecules and slow down their rotational dynamics (in Fig. 4C). The reorientation of water molecules plays a crucial role in the hydrogen bonding dynamics (48). The kinetics of making and breaking hydrogen bonds of ice-like water molecules in different PMETA-anion systems was also studied (see MD method and Fig. 4, D and E). The formation of ice-like water molecules is determined by the interplay between making rate constant (k) and breaking rate constant (k') of ice-like water. The transformation of water molecules from the liquid-like to the ice-like structure becomes more difficult when their rotational dynamics slows down because the neighboring water molecules need to adjust their positions and orientations to form an ice-like structure. In contrast, the breaking rate constants of ice-like water molecules (k') fluctuate slightly for all three systems (inset of Fig. 4D).

DISCUSSION

Recently, Tielrooij *et al.* (26) reported that the effect of cations and anions on water structure is nonadditive, exhibiting a long-range feature

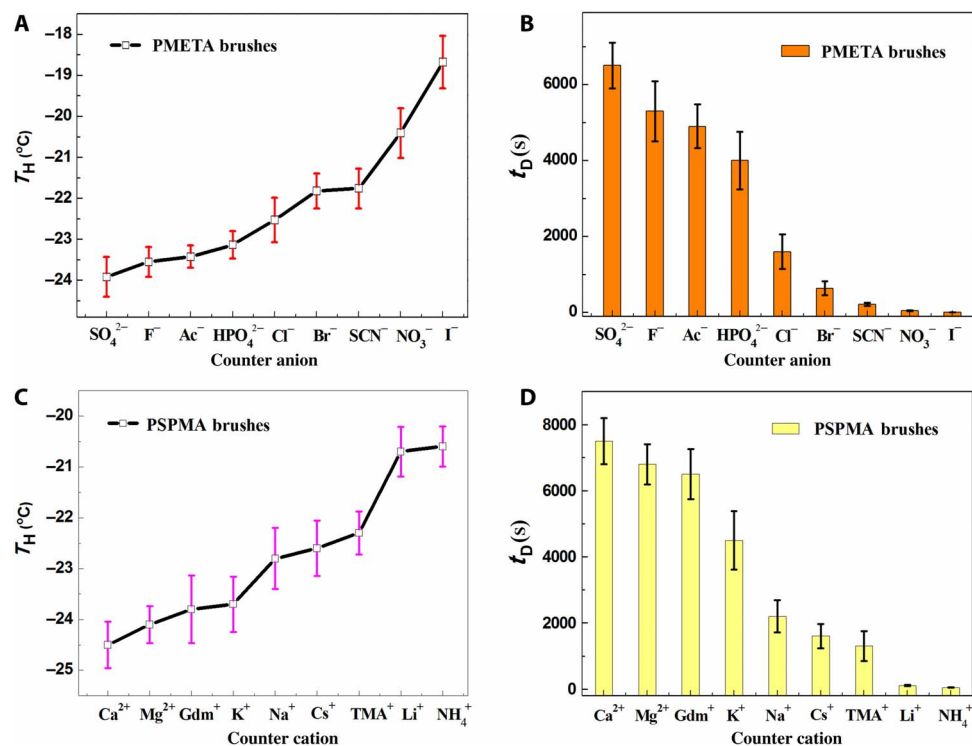


Fig. 3. Distinct efficiency of anions and cations in tuning HIN follows the Hofmeister series. (A and B) T_H (A) and t_D (B) on the PMETA brush surfaces with different counteranions follow the Hofmeister series. The brush grafting density is 0.50 chain/nm², and the thickness is 50 nm. (C and D) T_H (C) and t_D (D) of ice nucleation on PSPMA brushes with different counteranions. The brush grafting density is 0.95 chain/nm², and the thickness is 20 nm.

beyond the first hydration shell of ions. It was found that ions are not independent species in aqueous solutions, and ion-ion interactions are important. Collins (44) has proposed an empirical law of matching water affinities (LMWA). According to the LMWA, the oppositely charged ions tend to associate into compact ion pairs if their hydration free energies are close to each other (27, 28, 44). In particular, both the specific long-range electrostatic interactions between oppositely charged ions and the short-range hydration of ion pairs may strongly affect the dynamics and structure of the interfacial water.

We performed MD simulations to investigate the interactions between PMETA brushes and three representative counterions, F^- , Cl^- , and I^- . Because of excluded volume effect and electrostatic repulsion between the charged groups of the PB (36, 49), the PB chains are heavily stretched in water. At the same time, the dissociation of QA halide pairs occurs, and free halide ions diffuse to the brush/water interface, forming a counterion-rich interfacial water layer. According to the LMWA, the capability of F^- , Cl^- , and I^- to form compact ion pairs with the QA^+ group increases because the charge density decreases in the sequence of $\text{F}^- > \text{Cl}^- > \text{I}^-$ and the QA^+ ion has a low charge density. Thus, the concentrations of diffused counterions at the water/brush interfaces decrease in the order of $\text{F}^- > \text{Cl}^- > \text{I}^-$, which agrees well with the simulation results. When the grafting density or the thickness of the PB is higher, the electric field generated by the QA^+ groups is also stronger, which imposes higher attractive potential to the counterions and so prevents them from escaping into the brush/water interface. This effect is more evident for the weakly hydrated ions (here, I^-), which prefer to stay inside the PB due to the LMWA and so effectively amplify the difference, as shown in Fig. 2 (C and D).

The orientational relaxation of interfacial water molecules decays more slowly with the increase of the anion charge density, as shown in Fig. 4C. Meanwhile, the hydrogen bond making rate of ice-like water molecules increases in the order of $\text{F}^- < \text{Cl}^- < \text{I}^-$, whereas the difference of the hydrogen bond breaking rate of ice-like water molecules is minimal (see inset of Fig. 4D). Note that the hydrogen bond making rate and the fraction of ice-like water molecules, which were calculated through independent analysis from MD simulation (see MD method), follow the same increment trend as a function of the distance (within 15 Å) from the brush/water interface. This is in agreement with the classical relationship between the concentration and the rate constant in a dynamic equilibrium state, $C_{\text{ice-like water}}/C_{\text{liquid-like water}} = k/k'$. We also compared the fraction and the making rate constant of ice-like water molecules at the local brush/water interface with the same concentration of counterions (see table S1). The results in Fig. 4 (B and D) demonstrate the amplified ion-specific effect due to the increase of counterion concentration in the Hofmeister order. Consequently, the total numbers of ice-like water molecules on the surface of PMETA-I and PMETA-Cl are 8 and 6% higher than that on the PMETA-F surface. Because the rate of ice formation is strongly controlled by the fraction of ice-like water, HIN is more likely to occur on the brush surface with a low charge density counterion (here, PMETA-I) (19, 45). Also note that HIN is also influenced by the effective contact area between the water and the PB. For the PB with the same thickness and grafting density but different counterions (F^- , Cl^- , and I^-), the effective contact area is almost the same (figs. S15 and S18A). Therefore, the structure and dynamics of interfacial water dominate HIN. In contrast, the effective contact area increases with

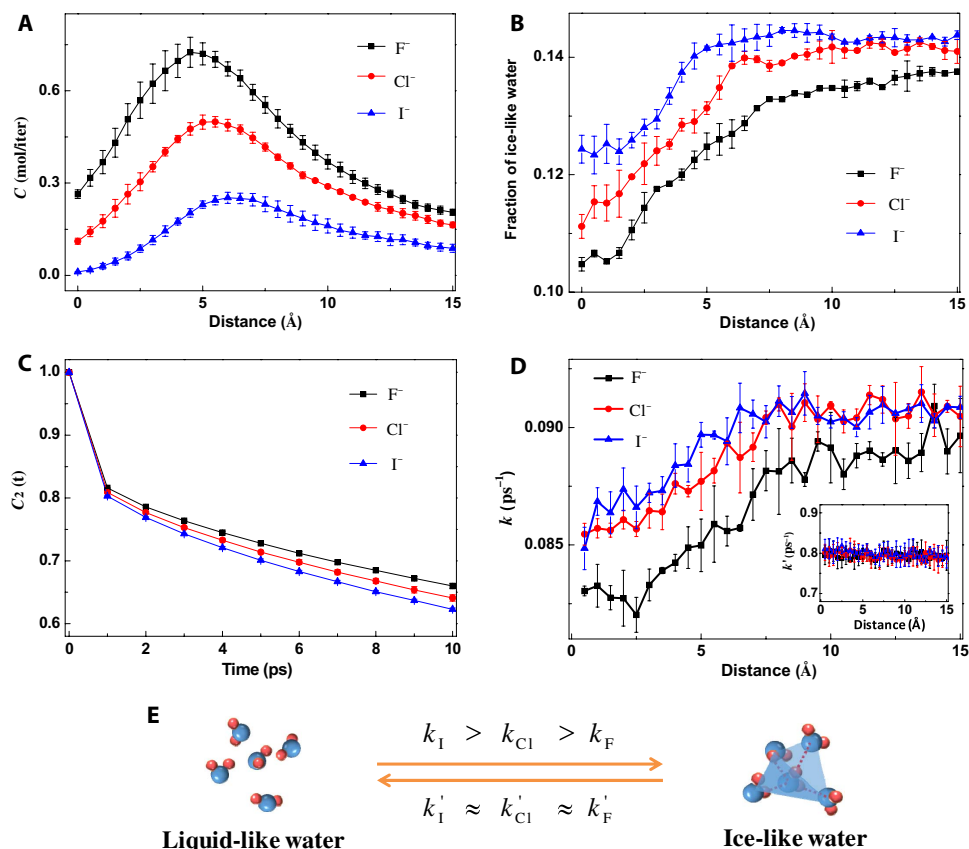


Fig. 4. The concentration of counteranions and the water structure and dynamics at the brush/water interfaces. (A) Concentration of diffused counteranions outside the PMETA brush. (B) Fraction of ice-like water molecules (tetrahedrality above 0.9). (C) Time correlation function of $-OH$ orientation of water molecules at a distance within 8 \AA from the brush/water interface. (D) Making rate constant and breaking rate constant (inset) of ice-like water molecules. (E) Kinetics of structural transformation between liquid-like and ice-like water molecules at the brush/water interface.

the grafting densities and/or thicknesses of the PB, which leads to an increased statistical probability of HIN. Consequently, the T_H increases, as shown in Fig. 2 (C and D). In principle, one can consider to characterize the HIN phenomenon by calculating the thermodynamic properties, such as enthalpy, entropy, and heat capacity in MD simulations. However, the complicated composition of the PB system and the nonequilibrium feature of the ice nucleation process make the interpretation of the results very difficult. Therefore, we will leave this for later study.

To our knowledge, these results are the first to show that ion specificity in tuning HIN on ionic surfaces follows the Hofmeister series. This finding not only shed new light on the ion-specific effect on ice nucleation but can also stimulate future studies involving the design of anti-icing material. The physical principle behind this work will further motivate the ongoing interest in exploring the origins of Hofmeister effects.

MATERIALS AND METHODS

Materials

Cationic PMETA and anionic PSPMA brushes were prepared on gold surface, modified by either initiator or methyl-terminated monolayers. The subsequent polymerizations were based on surface-initiated atom

transfer radical polymerization (SI-ATRP) in a 2:1 (v/v) oxygen-free water/methanol mixture. The samples were then washed with Milli-Q water and dried under N_2 flow. The different grafting densities of PMETA brushes were tuned by adjusting the mixing ratio of unreacted CH_3 -terminated functionalities and ATRP initiator. The grafting density (σ) is calculated by $\sigma = N_{Ap}h_{dry}/M_n$, where N_A is the Avogadro number, h_{dry} is the dry thickness of polymer measured by ellipsometer, M_n is the number average molecular weight, and ρ is the density of PMETA (1.0 g/cm^3) (50).

Counterions exchange

The Cl^- in PMETA and K^+ in PSPMA were exchanged by immersing the brushes into 0.1 M solutions of target counterions for 60 min. The samples were subsequently washed with Milli-Q water to remove excess surface free salt. The completeness of ion exchange was further confirmed by x-ray photoelectron spectroscopy (XPS) (fig. S1). Replacing the original Cl^- with I^- and SO_4^{2-} resulted in the appearance of new peaks of binding energies at 618.4 eV (I3d) and at 168.6 eV (S2p), whereas the signal of Cl^- at 196.7 eV (Cl2p) disappeared. The absence of the signal of Na^+ atom indicated that free salt inside the brushes has been removed.

Water freezing procedure

The T_H and t_D were measured by the homemade experimental apparatus (fig. S2). The sample cell was composed of a rubber O-ring sandwiched

between two cover glasses (42). The t_D of ice nucleation is defined as the time interval between the time when the substrate reaches a target temperature and the time when the ice nucleus appears. Water droplets can be deposited at -20.0°C (target temperature) for several hours without a noticeable water condensation or evaporation.

MD method

Sixteen (META)₁₂ polycation chains were homogeneously grafted perpendicular to a Si(1 0 0) surface, leading to a grafting density of 0.69 chains/nm². Counterions of F⁻, Cl⁻, and I⁻ (192) were added near QA⁺ groups to neutralize the system. Water molecules (18,551) were also added to each system. The force fields and simulation details of the brushes with different counterions are reported in the Supplementary Materials. The structural order parameter (tetrahedrality) of the interfacial water was calculated by

$$q_i = 1 - \frac{3}{8} \sum_{j=1}^3 \sum_{k=j+1}^4 \left(\cos \psi_{jik} + \frac{1}{3} \right)^2$$

where i represents the central water molecule, j and k represent the four nearest water molecules around water i , and ψ_{jik} is the angle formed by jik (51). We regard the water molecule with $q = 1$ to 0.9 as ice-like water ($q = 1$ corresponds to a water in a perfect tetrahedral ice crystal), which acts as the precursor of ice nucleus. The fraction of ice-like water (tetrahedrality above 0.9) in bulk water is about 14%. More simulation details are presented in the Supplementary Materials.

Water dynamics can be noted by water orientational time correlation functions (TCFs)

$$C_2(t) = \langle P_2[\mu_{\text{OH}}(0) \cdot \mu_{\text{OH}}(t)] \rangle$$

where P_2 is the second-order Legendre polynomial and μ_{OH} is the direction vector of the OH bond of water molecules. Similar to the calculation of the kinetics of hydrogen bonds in liquid water, we computed the time constants of the formation of ice-like water molecules (48). The function $p_i(t + t_0, t_0)$ is defined as 1 if the water molecule i is ice-like (liquid-like) during the time from t_0 to $t + t_0$, and within this interim, it does not transform into liquid-like (ice-like). Otherwise, it is defined as 0. The TCF $C(t)$ can be calculated from the simulation data

$$C(t) = \langle p_i(t + t_0, t_0) \rangle / \langle p_i(t_0, t_0) \rangle$$

It is assumed that $C(t)$ decays exponentially as

$$C(t) = \exp(-kt)$$

where k is the rate constant.

SUPPLEMENTARY MATERIALS

Supplementary material for this article is available at <http://advances.sciencemag.org/cgi/content/full/2/6/e1600345/DC1>

fig. S1. XPS spectra of PEMA brushes with different counterions (SO₄²⁻, Cl⁻, and I⁻) in the regions of S2p, Cl2p, and I3d.

fig. S2. Homemade experimental apparatus used to detect the HIN on PB surfaces.

fig. S3. Freezing process of individual water droplets on PMETA-I brushes (0.05 chain/nm²) during the temperature-jump experiment at a cooling rate of 2.0°C/min (detected by a high-speed camera).

fig. S4. Preparation process of PMETA-SO₄ and PMETA-I brush surfaces divided by a gap of Si on the same wafer.

fig. S5. Distribution of T_H on PMETA brush surfaces (grafting density of 0.5 chain/nm² and thickness of 50 nm) with different counterions (SO₄²⁻, Cl⁻, and I⁻).

fig. S6. HIN on cationic SAMs with different counteranions.

fig. S7. Influence of cooling rate (from 1.0 to 10.0°C/min) on the ice nucleation temperature of PMETA-SO₄, PMETA-Cl, and PMETA-I brush surfaces (grafting density of 0.5 chain/nm² and thickness of 50 nm).

fig. S8. Distribution of T_H on PSPMA brush surfaces (grafting density of 0.9 chain/nm² and thickness of 20 nm) with different counterions (Li⁺, Na⁺, and K⁺).

fig. S9. HIN on anionic SAMs with different counteranions.

fig. S10. Quartz crystal microbalance with dissipation monitoring results as a function of different counteranions in the PMETA brushes.

fig. S11. Thickness of PMETA brushes with different counterions measured by spectroscopic ellipsometer under aqueous solution.

fig. S12. Contact angle of PMETA brush surfaces with different counterions.

fig. S13. Surface morphology and roughness of PMETA brush.

fig. S14. MD simulation illustration of PB with counterions.

fig. S15. Distribution of outmost QA⁺ headgroup of PMETA-F, PMETA-Cl, and PMETA-I at the brush/water interface.

fig. S16. Concentration of the diffused counterions above the PMETA brush at 300 K.

fig. S17. Strength of the electric field of PMETA-F, PMETA-Cl, and PMETA-I above the brush/water interface.

fig. S18. Water density and ice-like water density of PMETA-F, PMETA-Cl, and PMETA-I brushes. table S1. The fraction of ice-like water molecules (tetrahedrality above 0.9), the ice-like water making rate constant k , and the concentration of ice-like water at the brush/water interface with the same concentration of counterion (0.25 M).

Experiment details

MD simulation details

References (52–58)

REFERENCES AND NOTES

1. K. Golovin, S. P. R. Kobaku, D. H. Lee, E. T. DiLoreto, J. M. Mabry, A. Tuteja, Designing durable icephobic surfaces. *Sci. Adv.* **2**, e1501496 (2016).
2. D. Ehre, E. Lavert, M. Lahav, I. Lubomirsky, Water freezes differently on positively and negatively charged surfaces of pyroelectric materials. *Science* **327**, 672–675 (2010).
3. M. Shimazu, A. Mulchandani, W. Chen, Cell surface display of organophosphorus hydrolase using ice nucleation protein. *Biotechnol. Prog.* **17**, 76–80 (2001).
4. A. Tabazadeh, Y. S. Djikaev, H. Reiss, Surface crystallization of supercooled water in clouds. *Proc. Natl. Acad. Sci. U.S.A.* **99**, 15873–15878 (2002).
5. T. Bartels-Rausch, Chemistry: Ten things we need to know about ice and snow. *Nature* **494**, 27–29 (2013).
6. D. T. Vaniman, D. L. Bish, S. J. Chipera, C. I. Fialips, J. W. Carey, W. C. Feldman, Magnesium sulphate salts and the history of water on Mars. *Nature* **431**, 663–665 (2004).
7. J. M. C. Plane, Cosmic dust in the earth's atmosphere. *Chem. Soc. Rev.* **41**, 6507–6518 (2012).
8. B. F. Ryan, The growth of ice parallel to the basal plane in supercooled water and supercooled metal fluoride solutions. *J. Cryst. Growth* **5**, 284–288 (1969).
9. B. F. Ryan, W. C. Macklin, The growth of ice in supercooled aqueous solutions. *J. Cryst. Growth* **2**, 337–340 (1968).
10. H. R. Pruppacher, On the growth of ice crystals in supercooled water and aqueous solution drops. *Pure Appl. Geophys.* **68**, 186–195 (1967).
11. J. Drzymala, Z. Sadowski, L. Holysz, E. Chibowski, Ice/water interface: Zeta potential, point of zero charge, and hydrophobicity. *J. Colloid Interface Sci.* **220**, 229–234 (1999).
12. H. Watanabe, T. Otsuka, M. Harada, T. Okada, Imbalance between anion and cation distribution at ice interface with liquid phase in frozen electrolyte as evaluated by fluorometric measurements of pH. *J. Phys. Chem. C* **118**, 15723–15731 (2014).
13. A. L. Becker, K. Henzler, N. Welsch, M. Ballauff, O. Borisov, Proteins and polyelectrolytes: A charged relationship. *Curr. Opin. Colloid In. Sci.* **17**, 90–96 (2012).
14. T. Kaasgaard, O. G. Mouritsen, K. Jørgensen, Freeze/thaw effects on lipid-bilayer vesicles investigated by differential scanning calorimetry. *Biochim. Biophys. Acta* **1615**, 77–83 (2003).
15. H. Kanno, C. A. Angell, Homogeneous nucleation and glass formation in aqueous alkali halide solutions at high pressures. *J. Phys. Chem.* **81**, 2639–2643 (1977).
16. H. R. Pruppacher, M. Neiburger, The effect of water soluble substances on the supercooling of water drops. *J. Atmos. Sci.* **20**, 376–385 (1963).
17. H. R. Pruppacher, Some relations between the supercooling and the structure of aqueous solutions. *J. Chem. Phys.* **39**, 1586–1594 (1963).

18. T. Koop, B. Luo, A. Tsias, T. Peter, Water activity as the determinant for homogeneous ice nucleation in aqueous solutions. *Nature* **406**, 611–614 (2000).
19. E. B. Moore, V. Molinero, Structural transformation in supercooled water controls the crystallization rate of ice. *Nature* **479**, 506–508 (2011).
20. A. Hudait, V. Molinero, Ice crystallization in ultrafine water–salt aerosols: Nucleation, ice-solution equilibrium, and internal structure. *J. Am. Chem. Soc.* **136**, 8081–8093 (2014).
21. A. Belitzky, E. Mishuk, D. Ehre, M. Lahav, I. Lubomirsky, Source of electrofreezing of supercooled water by polar crystals. *J. Phys. Chem. Lett.* **7**, 43–46 (2016).
22. J. P. D. Abbatt, S. Benz, D. J. Cziczo, Z. Kanji, U. Lohmann, O. Möhler, Solid ammonium sulfate aerosols as ice nuclei: A pathway for cirrus cloud formation. *Science* **313**, 1770–1773 (2006).
23. S. Nihonyanagi, S. Yamaguchi, T. Tahara, Counterion effect on interfacial water at charged interfaces and its relevance to the Hofmeister series. *J. Am. Chem. Soc.* **136**, 6155–6158 (2014).
24. O. Azzaroni, A. A. Brown, W. T. S. Huck, Tunable wettability by clicking counterions into polyelectrolyte brushes. *Adv. Mater.* **19**, 151–154 (2007).
25. A. W. Omta, M. F. Kropman, S. Woutersen, H. J. Bakker, Negligible effect of ions on the hydrogen-bond structure in liquid water. *Science* **301**, 347–349 (2003).
26. K. J. Tielrooij, N. Garcia-Araez, M. Bonn, H. J. Bakker, Cooperativity in ion hydration. *Science* **328**, 1006–1009 (2010).
27. W. Kunz, P. Lo Nostro, B. W. Ninham, The present state of affairs with Hofmeister effects. *Curr. Opin. Colloid In. Sci.* **9**, 1–18 (2004).
28. P. Jungwirth, P. S. Cremer, Beyond Hofmeister. *Nat. Chem.* **6**, 261–263 (2014).
29. A. Salis, B. W. Ninham, Models and mechanisms of Hofmeister effects in electrolyte solutions, and colloid and protein systems revisited. *Chem. Soc. Rev.* **43**, 7358–7377 (2014).
30. M. C. Pinna, P. Bauduin, D. Touraud, M. Monduzzi, B. W. Ninham, W. Kunz, Hofmeister effects in biology: Effect of choline addition on the salt-induced super activity of horseradish peroxidase and its implication for salt resistance of plants. *J. Phys. Chem. B* **109**, 16511–16514 (2005).
31. M. C. Pinna, A. Salis, M. Monduzzi, B. W. Ninham, Hofmeister series: The hydrolytic activity of *Aspergillus niger* lipase depends on specific anion effects. *J. Phys. Chem. B* **109**, 5406–5408 (2005).
32. V. S. J. Craig, Bubble coalescence and specific-ion effects. *Curr. Opin. Colloid In. Sci.* **9**, 178–184 (2004).
33. X. Chen, S. C. Flores, S.-M. Lim, Y. Zhang, T. Yang, J. Kherb, P. S. Cremer, Specific anion effects on water structure adjacent to protein monolayers. *Langmuir* **26**, 16447–16454 (2010).
34. X. Chen, T. Yang, S. Kataoka, P. S. Cremer, Specific ion effects on interfacial water structure near macromolecules. *J. Am. Chem. Soc.* **129**, 12272–12279 (2007).
35. J. T. O'Brien, J. S. Prell, M. F. Bush, E. R. Williams, Sulfate ion patterns water at long distance. *J. Am. Chem. Soc.* **132**, 8248–8249 (2010).
36. H. Ahrens, S. Förster, C. A. Helm, Charged polymer brushes: Counterion incorporation and scaling relations. *Phys. Rev. Lett.* **81**, 4172–4175 (1998).
37. Q. Wei, M. Cai, F. Zhou, W. Liu, Dramatically tuning friction using responsive polyelectrolyte brushes. *Macromolecules* **46**, 9368–9379 (2013).
38. M. A. C. Stuart, W. T. S. Huck, J. Genzer, M. Müller, C. Ober, M. Stamm, G. B. Sukhorukov, I. Szleifer, V. V. Tsukruk, M. Urban, F. Winnik, S. Zauscher, I. Luzinov, S. Minko, Emerging applications of stimuli-responsive polymer materials. *Nat. Mater.* **9**, 101–113 (2010).
39. M. Schrinner, M. Ballauff, Y. Talmon, Y. Kauffmann, J. Thun, M. Möller, J. Breu, Single nanocrystals of platinum prepared by partial dissolution of Au-Pt nanoalloys. *Science* **323**, 617–620 (2009).
40. M. Chen, W. H. Briscoe, S. P. Armes, J. Klein, Lubrication at physiological pressures by polyelectrolyte brushes. *Science* **323**, 1698–1701 (2009).
41. M. Ballauff, Spherical polyelectrolyte brushes. *Prog. Polym. Sci.* **32**, 1135–1151 (2007).
42. K. Li, S. Xu, W. Shi, M. He, H. Li, S. Li, X. Zhou, J. Wang, Y. Song, Investigating the effects of solid surfaces on ice nucleation. *Langmuir* **28**, 10749–10754 (2012).
43. F. Rodriguez-Ropero, N. F. A. van der Vegt, Ionic specific effects on the structure, mechanics and interfacial softness of a polyelectrolyte brush. *Faraday Discuss.* **160**, 297–309 (2013).
44. K. D. Collins, M. W. Washabaugh, The Hofmeister effect and the behaviour of water at interfaces. *Q. Rev. Biophys.* **18**, 323–422 (1985).
45. M. Matsumoto, S. Saito, I. Ohmine, Molecular dynamics simulation of the ice nucleation and growth process leading to water freezing. *Nature* **416**, 409–413 (2002).
46. I. M. Svishchev, P. G. Kusalik, Electrofreezing of liquid water: A microscopic perspective. *J. Am. Chem. Soc.* **118**, 649–654 (1996).
47. L. Lupi, A. Hudait, V. Molinero, Heterogeneous nucleation of ice on carbon surfaces. *J. Am. Chem. Soc.* **136**, 3156–3164 (2014).
48. A. Luzar, D. Chandler, Hydrogen-bond kinetics in liquid water. *Nature* **379**, 55–57 (1996).
49. A. Deshkovski, S. Obukhov, M. Rubinstein, Counterion phase transitions in dilute polyelectrolyte solutions. *Phys. Rev. Lett.* **86**, 2341–2344 (2001).
50. M. Kobayashi, M. Terada, Y. Terayama, M. Kikuchi, A. Takahara, Direct synthesis of well-defined poly[[2-(methacryloyloxy)ethyl]trimethylammonium chloride] brush via surface-initiated atom transfer radical polymerization in fluoroalcohol. *Macromolecules* **43**, 8409–8415 (2010).
51. J. R. Errington, P. G. Debenedetti, Relationship between structural order and the anomalies of liquid water. *Nature* **409**, 318–321 (2001).
52. H. J. C. Berendsen, J. R. Grigera, T. P. Straatsma, The missing term in effective pair potentials. *J. Phys. Chem.* **91**, 6269–6271 (1987).
53. M. J. Frisch, G. W. Trucks, H. B. Schlegel, G. E. Scuseria, M. A. Robb, J. R. Cheeseman, G. Scalmani, V. Barone, B. Mennucci, G. A. Petersson, H. Nakatsuji, M. Caricato, X. Li, H. P. Hratchian, A. F. Izmaylov, J. Bloino, G. Zheng, J. L. Sonnenberg, M. Hada, M. Ehara, K. Toyota, R. Fukuda, J. Hasegawa, M. Ishida, T. Nakajima, Y. Honda, O. Kitao, H. Nakai, T. Vreven, J. A. Montgomery Jr., J. E. Peralta, F. Ogliaro, M. Bearpark, J. J. Heyd, E. Brothers, K. N. Kudin, V. N. Staroverov, R. Kobayashi, J. Normand, K. Raghavachari, A. Rendell, J. C. Burant, S. S. Iyengar, J. Tomasi, M. Cossi, N. Rega, J. M. Millam, M. Klene, J. E. Knox, J. B. Cross, V. Bakken, C. Adamo, J. Jaramillo, R. Gomperts, R. E. Stratmann, O. Yazyev, A. J. Austin, R. Cammi, C. Pomelli, J. W. Ochterski, R. L. Martin, K. Morokuma, V. G. Zakrzewski, G. A. Voth, P. Salvador, J. J. Dannenberg, S. Dapprich, A. D. Daniels, Ö. Farkas, J. B. Foresman, J. V. Ortiz, J. Cioslowski, and D. J. Fox, Gaussian 09, Revision A.02. Gaussian Inc., Wallingford, CT (2009).
54. J. Wang, R. M. Wolf, J. W. Caldwell, P. A. Kollman, D. A. Case, Development and testing of a general amber force field. *J. Comput. Chem.* **25**, 1157–1174 (2004).
55. I. S. Joung, T. E. Cheatham III, Determination of alkali and halide monovalent ion parameters for use in explicitly solvated biomolecular simulations. *J. Phys. Chem. B* **112**, 9020–9041 (2008).
56. I. Leontyev, A. Stuchebrukhov, Accounting for electronic polarization in non-polarizable force fields. *Phys. Chem. Chem. Phys.* **13**, 2613–2626 (2011).
57. D. A. Case *et al.*, AMBER 12. University of California, San Francisco, CA (2012).
58. J.-P. Ryckaert, G. Cicotti, H. J. C. Berendsen, Numerical integration of the Cartesian equations of motion of a system with constraints: Molecular dynamics of *n*-alkanes. *J. Comput. Phys.* **23**, 327–341 (1977).

Acknowledgments: We thank R. Dou for the initial test. **Funding:** This work was supported by the 973 Program (2012CB933801 and 2013CB933004) and the National Natural Science Foundation of China (51436004, 21421061, and 2150030233). **Author contributions:** J.W. initiated the idea of investigating the effect of ions on HIN with PB surfaces and supervised the experiments. Y.Q.G. supervised the MD simulation. Z.H. and Z.L. designed and carried out the experiments. W.J.X. carried out the MD simulation. Z.H., W.J.X., and J.W. wrote the initial draft of the manuscript. Z.W. and G.L. contributed to the analysis of the data. **Competing interests:** The authors declare that they have no competing interests. **Data and materials availability:** All data needed to evaluate the conclusions in the paper are present in the paper and/or the Supplementary Materials. Additional data related to this paper may be requested from the authors.

Submitted 18 February 2016

Accepted 12 May 2016

Published 3 June 2016

10.1126/sciadv.1600345

Citation: Z. He, W. J. Xie, Z. Liu, G. Liu, Z. Wang, Y. Q. Gao, J. Wang, Tuning ice nucleation with counterions on polyelectrolyte brush surfaces. *Sci. Adv.* **2**, e1600345 (2016).

Tuning ice nucleation with counterions on polyelectrolyte brush surfaces

Zhiyuan He, Wen Jun Xie, Zhenqi Liu, Guangming Liu, Zuowei Wang, Yi Qin Gao and Jianjun Wang

Sci Adv 2 (6), e1600345.

DOI: 10.1126/sciadv.1600345

ARTICLE TOOLS

<http://advances.sciencemag.org/content/2/6/e1600345>

SUPPLEMENTARY MATERIALS

<http://advances.sciencemag.org/content/suppl/2016/05/31/2.6.e1600345.DC1>

REFERENCES

This article cites 56 articles, 8 of which you can access for free
<http://advances.sciencemag.org/content/2/6/e1600345#BIBL>

PERMISSIONS

<http://www.sciencemag.org/help/reprints-and-permissions>

Use of this article is subject to the [Terms of Service](#)